

# NTK-Guided Few-Shot Class Incremental Learning

Jingren Liu, Zhong Ji, *Senior Member, IEEE*, Yanwei Pang, *Senior Member, IEEE*, YunLong Yu

**Abstract**—While anti-amnesia FSCIL learners often excel in incremental sessions, they tend to prioritize mitigating knowledge attrition over harnessing the model’s potential for knowledge acquisition. In this paper, we delve into the foundations of model generalization in FSCIL through the lens of the Neural Tangent Kernel (NTK). Our primary design focus revolves around ensuring optimal NTK convergence and NTK-related generalization error, serving as the theoretical bedrock for exceptional generalization. To attain globally optimal NTK convergence, we employ a meta-learning mechanism grounded in mathematical principles to guide the optimization process within an expanded network. Furthermore, to reduce the NTK-related generalization error, we commence from the foundational level, optimizing the relevant factors constituting its generalization loss. Specifically, we initiate self-supervised pre-training on the base session to shape the initial network weights. Then they are carefully refined through curricular alignment, followed by the application of dual NTK regularization tailored specifically for both convolutional and linear layers. Through the combined effects of these measures, our network acquires robust NTK properties, significantly enhancing its foundational generalization. On popular FSCIL benchmark datasets, our NTK-FSCIL surpasses contemporary state-of-the-art approaches, elevating end-session accuracy by 2.9% to 8.7%.

**Index Terms**—Few-shot Class-Incremental Learning, Neural Tangent Kernel, Generalization, Self-supervised Learning.

## I. INTRODUCTION

Few-shot class-incremental learning (FSCIL) extends class-incremental learning (CIL) by facilitating the continuous learning of incremental classes with only a few data samples. Drawing inspiration from established CIL approaches [1]–[3], contemporary FSCIL methods [4]–[7] primarily emphasize safeguarding the pre-established knowledge in every session, specifically addressing the catastrophic forgetting problem. In contrast to CIL, which undergoes training in every session, the FSCIL learner is exclusively trained in the base session. Parameter updates for the FSCIL learner do not occur during subsequent incremental sessions. Consequently, the effectiveness of the subsequent incremental sessions relies heavily on the generalization capabilities developed during the training of the base session. Despite its significance, the emphasis

on model generalization has been somewhat overlooked in existing FSCIL literature. To address this gap, we introduce the concept of the “Neural Tangent Kernel (NTK)” and highlight its pivotal role in understanding the generalization properties of neural networks in the FSCIL context.

*Definition 1 (Neural Tangent Kernel):* For a typical ConvNet with randomly initialized parameters  $\theta_0$ , NTK is given by  $\Phi_0(x, x') = \left\langle \frac{\partial f(\theta_0, x)}{\partial \theta_0}, \frac{\partial f(\theta_0, x')}{\partial \theta_0} \right\rangle$ , and it converges to a fixed kernel as the width  $l$  approaches infinity and the different inputs  $x$  and  $x'$  undergo constant alteration,

$$\Phi(\cdot) = \lim_{l \rightarrow \infty} \Phi_0(\cdot), \quad (1)$$

where  $f$  denotes the neural network,  $\frac{\partial f(\theta, \cdot)}{\partial \theta}$  is the neural network jacobian [8],  $\Phi(\cdot)$  signifies the fully converged NTK matrix and  $l$  indicates the model’s width.

A fundamental insight from the NTK corpus posits that *increasing the network’s width tends to facilitate the NTK’s convergence to a stable matrix during optimization, thereby bolstering generalization capabilities*. This phenomenon suggests that post-optimization, the outputs of a network with infinite width become robust to variations in parameters and inputs, effectively capturing the inherent structures of the input data to produce reliable and consistent outputs for both familiar and novel data. Such a mechanism significantly mitigates the risk of overfitting, enhancing the model’s aptitude for generalizing to unseen data and advancing it towards an ideal state of generalization.

As emphasized in Definition 1, it’s noted that incrementally broadening the network width simplifies the path to NTK convergence, diminishing the reliance on manual tuning during the NTK optimization process. However, it’s imperative to acknowledge that even before achieving a theoretically infinite width, manual interventions may be necessary, often incurring considerable computational demands as delineated in preceding research. For instance, the work by [9] underscores the computational intensity of computing the NTK for randomized data through ConvNets, requiring up to 200 gigabytes of GPU memory, thus posing a substantial challenge for a wide array of applications. Moreover, while the concept of an infinitely wide network is conceptually appealing, its practical application remains constrained by real-world limitations.

Therefore, incorporating NTK into FSCIL presents the challenge of ensuring that a finite-width network exhibits NTK properties akin to those of an infinitely wide network, even with limited optimization resources. Ideally, an infinitely wide network would demonstrate both excellent NTK convergence [10]–[12] and a generalization loss approaching zero after optimization [11], [13]–[15]. Our goal is to replicate these properties within the constraints of a finite-width network.

This work was supported by the National Key Research and Development Program of China (Grant No. 2022ZD0160403), and the National Natural Science Foundation of China (NSFC) under Grant 62176178 (Corresponding author: Zhong Ji).

Zhong Ji and Yanwei Pang are with the School of Electrical and Information Engineering, Tianjin Key Laboratory of Brain-Inspired Intelligence Technology, Tianjin University, Tianjin 300072, China, and also with the Shanghai Artificial Intelligence Laboratory, Shanghai 200232, China (e-mail: jizhong@tju.edu.cn; pyw@tju.edu.cn).

Jingren Liu is with the School of Electrical and Information Engineering, Tianjin Key Laboratory of Brain-Inspired Intelligence Technology, Tianjin University, Tianjin 300072, China (e-mail: jrl0219@tju.edu.cn).

YunLong Yu is with the College of Information Science and Electronic Engineering, Zhejiang University, Hangzhou, 310027, China. (e-mail: yuyunlong@zju.edu.cn).

Guided by these insights, our work focuses on addressing two critical issues—**NTK Convergence** and **NTK Generalization**—and seamlessly integrating them within the FSCIL framework. These methods are approached through the lens of the equivalence between meta-learning optimization and NTK convergence from Theorem 1 and Theorem 2, as well as through the NTK-related generalization loss in Theorem 3.

To achieve NTK convergence in our expanded network during optimization, we theoretically align NTK convergence with meta-learning optimization. This alignment is based on the understanding that both meta-loss and meta-outputs are intrinsically linked to the NTK matrix and labels. Ensuring effective meta-learning performance in FSCIL is pivotal for attaining optimal NTK convergence. Consequently, we propose a bespoke meta-learning strategy for FSCIL task, aiming to ensure that initiating meta-training from scratch leads to foundational FSCIL performance.

Simultaneously, to ensure optimal NTK dynamics and minimal generalization loss, we incorporate self-supervised pre-training weights, curricular alignment, and dual NTK regularization, in line with [16] and the FSCIL guidelines. These strategies are chosen for their effectiveness in Eq. (3) and Theorem 3. In the regularization segment, to reduce computational overhead, we decompose the ConvNet and apply spectral regularization in convolutional layers [16]. For the additional linear layers, we directly compute the NTK matrix and impose a spectral constraint to its eigenvalues, compressing their distribution to render it more consolidated.

In a nutshell, our contributions are threefold:

- To the best of our knowledge, our work is the first to integrate NTK with FSCIL, advancing model generalization through robust theoretical foundations.
- To establish foundational NTK convergence during the FSCIL optimization, we theoretically align NTK convergence with meta-learning optimization and propose a bespoke meta-learning schema specifically tailored for the FSCIL task, initializing meta-training from scratch.
- Furthermore, to harvest optimal NTK dynamic outputs and the smallest NTK-related generalization loss, drawing inspiration from [16]–[19], we employ self-supervised pre-training, curricular alignment, and dual NTK regularization to achieve state-of-the-art results both theoretically and empirically.

## II. RELATED WORKS

**Neural Tangent Kernel.** It is initially proposed in [20], which reveals the relationship between the convergence of infinitely wide neural networks and model generalization. Continuing this pioneering work, subsequent studies [21], [22] further extend these findings to the case of shallow neural networks. Furthermore, recent works [11], [13]–[15] on highly over-parameterized neural networks show that gradient descent can achieve zero training error even for finite but sufficiently wide CNNs, revealing promising generalization potential. For example, [13], [23] elucidate the correlation between network width and generalization, demonstrating that over-parameterization and random initialization enable models

to converge linearly to the global minimum. Zhu *et al.* [15] show that over-parameterized wide networks can fit samples in polynomial time. Moreover, Bombari *et al.* [18] discuss model stability, feature alignment and their relation to generalization error. Diverging from these typical NTK approaches, our work seeks to further integrate FSCIL with NTK dynamics and improve generalization capabilities.

**Few-shot Class-Incremental Learning.** It is proposed to address CIL in few-shot context. In general, the current FSCIL approaches [24]–[26] principally are alleviating catastrophic forgetting in incremental sessions. For example, TOPIC [24] is the pioneer, which leverages neural gas structure to solidify knowledge. CEC [4] employs episodic training via a context-propagated graph model to enhance adaptability. Moreover, MCNet [27] introduces ensemble learning to complement different memorized knowledge. Building upon these foundations, subsequent methods [6], [7], [28], [29] have advanced via the class extension techniques, which is to preemptively prevent forgetting in future classes. For example, considered from forward compatibility, Zhou *et al.* [28] assign virtual prototypes to preserve space for incremental classes. ALICE [29] extends the virtual classes to limit and facilitates well-clustered features via sophisticate-designed loss. Compared to them, our NTK-FSCIL focuses more on the model generalization and alleviates catastrophic forgetting from the side.

## III. NTK THEORETICAL FOUNDATION IN FSCIL

### A. FSCIL Problem Formulation

In a dynamic training environment featuring  $N$  supervised tasks,  $\Upsilon_{t=1}^N$ , the essence of FSCIL is the incremental learning of these tasks without overlap. Specifically, the class sets  $\Upsilon_i$  and  $\Upsilon_j$  are disjoint for all  $i \neq j$ . The base session (session 0) provides an extensive dataset, while subsequent incremental sessions offer only a limited number of samples. Each task  $\Upsilon_t$  is configured in the  $n$ -way  $m$ -shot  $k$ -query setting for meta-training, represented as:

$$\Upsilon_t = (\mathbf{X}_i, \mathbf{X}_j, \mathbf{Y}_i, \mathbf{Y}_j),$$

The pair  $[\mathbf{X}_i, \mathbf{Y}_i] \in \mathbb{R}^{m \times h \times w \times c}, \mathbb{R}^{m \times p}$  signifies  $m$  support samples along with their corresponding labels. Here,  $h$ ,  $w$  and  $c$  denote the image’s dimensional indices, while  $p$  is the dimension of the one-hot encoded labels. Similarly, the pair  $[\mathbf{X}_j, \mathbf{Y}_j] \in \mathbb{R}^{k \times h \times w \times c}, \mathbb{R}^{k \times p}$  represents  $k$  query samples associated with their labels. Moreover,  $[X_i^t, Y_i^t]$  and  $[X_j^t, Y_j^t]$  are all support and query samples in task  $t$ .

### B. NTK Dynamics in FSCIL

Within the realm of NTK theory, foundational works by [10], [30] have illuminated the operational dynamics of fully connected neural networks, structured as delineated below:

$$u_l = \frac{\sigma_w W_l h_{l-1}}{\sqrt{Z_{l-1}}} + \sigma_b b_l, \quad h_l = \text{Relu}(u_l) \quad (l = 1, \dots, L), \quad (2)$$

with  $W_l \in \mathbb{R}^{Z_l \times Z_{l-1}}$  and  $b_l \in \mathbb{R}^{Z_l}$  denoting weight matrices and bias vectors initialized via  $\mathcal{N}(0, 1)$ .

In the infinite-width limit ( $Z_l \rightarrow \infty$ ), with finite samples and depth, gradient descent targets a global minimum, encapsulating the NTK regime. This regime in FSCIL yields the model for any input  $x$  as:

$$f(x) = f_0^*(x) + \Phi(x, X)(\Phi(X, X) + \lambda I)^{-1}(Y - f_0^*(X)). \quad (3)$$

Here,  $f_0^*(x)$  represents the model's initial weights.  $\Phi$  represents the NTK matrix for the base session, with  $x$  denoting an individual sample and  $X$  embodying the aggregated dataset specific to the base session.

**Remark:** The NTK is applicable across various architectures, including ResNets and Transformers [31], with the primary distinctions manifesting in the NTK matrix structure.

### C. Generalization and NTK Analysis

To mathematically capture the essence of model generalization in FSCIL, we adapt Theorem 1 and Theorem 2 from [11], alongside the Theorem 3 from [32].

**Theorem 1 (NTK-related Meta-Learning Output):** Assuming negligible learning rates  $\eta$  and  $\lambda$ , and given a network width  $l$  approaching infinity, the meta-outputs  $F_t$  for inputs  $\mathbf{X}_j \in \mathbf{X}_j^t$ , in relation to the training pairs  $(\mathbf{X}_i, \mathbf{Y}_i) \in (\mathbf{X}_i^t, \mathbf{Y}_i^t)$ , are highly likely to converge to a state describable by the NTK after optimization:

$$F_t(\mathbf{X}_j, \mathbf{X}_i, \mathbf{Y}_i) = G_{\Phi}^{\tau}(\mathbf{X}_j, \mathbf{X}_i, \mathbf{Y}_i) + \Phi((\mathbf{X}_j, \mathbf{X}_i), (\mathbf{X}_j^t, \mathbf{X}_i^t))T_{\Phi}^{\eta}(t)(\mathbf{Y}_j^t - G_{\Phi}^{\tau}(\mathbf{X}_j^t, \mathbf{X}_i^t, \mathbf{Y}_i^t)), \quad (4)$$

$$\tilde{T}_{\Phi}^{\lambda}(\cdot, \tau) = \Phi(\cdot, \cdot)^{-1}(I - e^{-\lambda\Phi(\cdot, \cdot)\tau}), \quad (5)$$

$$G_{\Phi}^{\tau}(\mathbf{X}_j, \mathbf{X}_i, \mathbf{Y}_i) = \Phi(\mathbf{X}_j, \mathbf{X}_i)\tilde{T}_{\Phi}^{\lambda}(\mathbf{X}_i, \tau)\mathbf{Y}_i, \quad (6)$$

where  $\Phi((\mathbf{X}_j, \mathbf{X}_i), (\mathbf{X}_j^t, \mathbf{X}_i^t))$  is a kernel function.

**Theorem 2 (NTK-related Meta-Learning Convergence):** Define NTK matrix  $\Phi = \lim_{l \rightarrow \infty} \frac{1}{l} J(\theta_0)J(\theta_0)^T$  and learning rate  $\eta_0 = \frac{2}{\sigma_{\min}(\Phi) + \sigma_{\max}(\Phi)}$ . In a randomly initialized ConvNet of progressive width  $l$ , for any infinitesimal positive  $\delta > 0$ , there exist positive real numbers  $R$  and  $\lambda_0$  such that an upper bound on the training loss is assuredly maintained with a probability exceeding  $1 - \delta$ .

$$\begin{aligned} \mathcal{L}(\theta_t) &= \frac{1}{2} \|F_{\theta_t}(\mathbf{X}_i, \mathbf{X}_j, \mathbf{Y}_i) - \mathbf{Y}_j\|_2^2 \\ &\leq \left(1 - \frac{\eta_0 \sigma_{\min}(\Phi)}{3}\right)^{2t} \frac{R^2}{2}. \end{aligned} \quad (7)$$

**Theorem 3 (NTK-related Generalization):** In the realm of FSCIL, for the base session, there exists an optimal function  $f^*(x)$ , fundamentally influenced by the spectral characteristics of the NTK. The expected generalization loss  $L_D(f^*)$  is dictated by these spectral properties and can be quantified as:

$$L_D(f^*) = \frac{1}{1 - \varepsilon} \sum_{i=0}^{\infty} \lambda_i w_i^{*2} \left(\frac{\beta}{\beta + N\lambda_i}\right)^2 + \frac{\varepsilon}{1 - \varepsilon} \sigma^2, \quad (8)$$

where  $\beta$  represents a numerically determined parameter,  $\varepsilon$  is a function of the eigenvalues  $\lambda_i$  of the NTK as well as the sample size  $N$ , and  $w_i^*$  symbolize the optimal weights corresponding to the deconstructed NTK in RKHS. The  $\beta$  and  $\varepsilon$  satisfy the relations outlined in the subsequent equations:

$$\sum_{i=0}^{\infty} \frac{\lambda_i}{\beta + N\lambda_i} = 1, \quad \sum_{i=0}^{\infty} \frac{N\lambda_i^2}{(\beta + N\lambda_i)^2} = \varepsilon. \quad (9)$$

From the insights provided in Eq. (3), it becomes clear that the pivotal factors influencing the optimization process during the base session are the initial weights  $f_0^*(x)$  and the alignment of logits  $Y - f_0^*(X)$ . To address these critical elements, we adopt self-supervised pre-training alongside curricular alignment as strategies for augmentation.

Ensuring optimal NTK convergence during the dynamic optimization phase necessitates establishing a mathematical equivalence between NTK convergence and meta-learning optimization within the context of FSCIL. Drawing upon Theorem 2, we ascertain that the meta-outputs and meta-loss are significantly influenced by the eigenvalue distribution of the NTK. This realization underscores the importance of fostering meta-learning optimization to facilitate NTK convergence, as highlighted in seminal works by [10]–[12]. Consequently, Subsec. IV is dedicated to elucidating strategies through which the FSCIL learner can surmount prevailing obstacles and achieve convergence within the meta-learning paradigm.

To minimize the generalization loss towards zero within the Reproducing Kernel Hilbert Space (RKHS), it is recognized that an optimal generalization loss depends on both the sample quantity and a stable eigenvalue spectrum [33], [34]. The formula  $\sum_{i=0}^{\infty} \lambda_i w_i^{*2} \left(\frac{\beta}{\beta + N\lambda_i}\right)^2$  underscores that an eigenvalue's  $\lambda_i$  impact on generalization loss is adjusted by its multiplication with the corresponding optimal weight  $w_i^*$ . This setup implies that larger eigenvalues, when coupled with larger weights, can significantly contribute to increased loss, whereas the influence of smaller eigenvalues is comparably minimal. Achieving uniformity in the NTK's eigenvalues — thereby avoiding extremes — ensures a more equitable contribution across all eigenvalues, mitigating any disproportionate effects on the total generalization loss. This balance is crucial for overall loss reduction.

In general, enhancing the number of base class samples and carefully moderating NTK eigenvalues are pivotal strategies for lowering generalization loss. We adopt the strategy of enlarging virtual class samples alongside dual NTK regularization to achieve this goal. These strategic measures collectively fortify the FSCIL learner's generalization efficiency, securing top-tier performance both theoretically and practically during the base session optimization.

## IV. META-LEARNING CONVERGENCE IN FSCIL

As delineated in Theorem 1 and Theorem 2, it is evident that the NTK governs the trajectory of meta-outputs during meta-training, with the NTK matrix's eigenvalue distribution shaping the meta-loss for backpropagation optimization. Thus, when optimizing meta-loss through gradient descent, the NTK is bound to achieve global convergence. At this point, NTK convergence is equated to meta-learning optimization.

Grounded in the established equivalence between NTK convergence and meta-learning optimization, we endeavor to steer FSCIL's meta-learning towards global optimal convergence, thereby ensuring the NTK's convergence to its optimal region. However, many existing FSCIL methods [4], [5], [28], [35] argue that initiating meta-learning from scratch often fails to converge to the global optimum, leading to suboptimal

FSCIL performance. To find the reasons of this performance degradation, we conduct a comprehensive study of the engineering implementations of existing methods. From this study, we identify two primary causes: (1) the inflexibility in logit combinations, and (2) the oversight of scenarios similar to incremental sessions during training.

In response to the aforementioned two reasons, we reformulate the classification loss, dividing it into two distinct facets as depicted in Eq. 10. The first component integrates the mixup mechanism with a superior margin-based loss (elaborated in Subsec. V-B), addressing the rigid class-level combinations during meta-training. Simultaneously, the second component introduces an unsupervised few-shot loss to simulate testing operations and enhance adaptability to scenarios similar to incremental sessions during training.

$$\mathcal{L}_{cls} = \underbrace{\mathcal{L}_{logits}}_{\text{Margin-based Loss}} + \gamma \underbrace{\mathcal{L}_{embeddings}}_{\text{Adaptability Loss}} \quad (10)$$

To mitigate the constraints of rigid class-level combinations during meta-training, inspired by [28], [29], we deploy a mixup strategy<sup>1</sup>. This mixup strategy, by virtually expanding class boundaries, facilitates the generation of highly diverse logits for virtual and real classes. Such an expansion is crucial for overcoming the rigid optimization inherent in scenarios with limited logit variability.

In prior meta-learning paradigms [4], [35], supervised pre-training and meta-learning refinement are typically performed across the entire class domain, generating associated logits. However, these methods often overlook the embedding-based classification method specific to each meta-task subspace, designed to simulate testing operations in incremental sessions. To address this, we deploy an unsupervised few-shot loss to better simulate and adapt to incremental session scenarios. Diverging from traditional methods, we reconfigure class indices in each batch to define sub-domain labels  $\mathbf{y}^*$ , and utilize embeddings-derived prototypes to generate pseudo-labels  $\mathbf{pl}$ .

$$\mathbf{pl} = \frac{\mathbf{X}_j \cdot \Omega_n \left( \frac{1}{m} \sum_{i=1}^m \mathbf{X}_i \right)}{\|\mathbf{X}_j\|_2 \cdot \|\Omega_n \left( \frac{1}{m} \sum_{i=1}^m \mathbf{X}_i \right)\|_2}, \quad (11)$$

where  $n$  and  $m$  denote their quantities in the  $n$ -way,  $m$ -shot scenario, and  $\Omega_n$  is the operation converging  $n$  prototypes.

After generating pseudo-labels in the sub-domain, we employ the classic cross-entropy loss to formulate the adaptability loss, denoted as  $\mathcal{L}_{embeddings} = CE(\mathbf{pl}, \mathbf{y}^*)$ .

Ultimately, by employing the mixup strategy to diversify class-level logit combinations and incorporating an adaptability loss to simulate incremental scenarios, our bespoke meta-learning strategy can directly start meta-training from scratch and omit the pre-training process, outperforming the conventional multi-step paradigm in performance and efficiency. Additionally, assisted by meta-learning, our NTK matrix theoretically reaches the global optimal convergence.

## V. REDUCING GENERALIZATION LOSS IN FSCIL

Drawing inspiration from Theorem 3 and [16], [18], [19], [36], we consider NTK-related dynamics and generalization

<sup>1</sup>See Sec. VI-E for an in-depth examination of various mixup strategies and their impact on FSCIL performance.

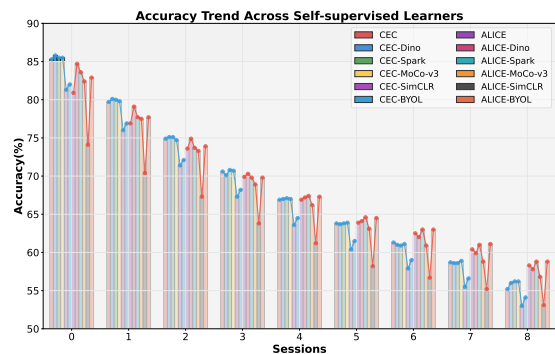


Fig. 1: The difference in FSCIL performance amongst various self-supervised learners, utilizing ResNet-18×2 on CIFAR100.

loss. In this literature, a more stable eigenvalue distribution of NTK matrix indicates a better generalization state, emphasizing the importance of real-time monitoring and constraining of the NTK’s eigenvalue distribution. Moreover, following the ideas from Eq. (3) and [16], [18], we understand that utilizing pre-trained models to initialize the model weights, combined with better logit-label alignment, will effectively optimize the NTK dynamic outputs, enhancing the model generalization capabilities. Thus, in this section, our exploration will focus on three facets: **initialization**, **alignment** and **regularization**.

### A. Initialize Weights: Self-Supervised Pre-Training

As highlighted in Eq. (3) and [16], pre-trained models significantly enhance model generalization and stabilize eigenvalue decay in NTK matrix. Yet, in FSCIL, using larger datasets for pre-training is often discouraged due to the risk of excessively enhancing the FSCIL learner’s generalization capabilities, which could potentially overshadow the challenges inherent in continual and few-shot scenarios. Adhering to FSCIL guidelines, we opt for self-supervised pre-training on the base session for effective initialization. To further investigate the impact of various self-supervised methods on FSCIL, we conduct experiments using two mainstream frameworks, CEC [4] and ALICE [29], and apply weights trained on the base session from self-supervised methods such as SwAV [37], Dino [38], SimCLR [39], SimSiam [40], MAE [41], MoCo-v3 [42], BYOL [43] and SparK [44]. The details and results are meticulously presented in Sec. VI-C and Fig. 1.

As evidenced in Fig. 1, the generative SparK framework [44] outperforms its contrastive learning-based counterparts. When the FSCIL learner is initialized with SparK’s weights, we observe notable improvements in incremental session accuracies, alongside maintained base session accuracy, which is indicative of enhanced generalization potential. Furthermore, as detailed in Sec. VI-H, the NTK’s eigenvalue distribution with SparK initialization demonstrates greater stability. Therefore, due to its excellent performance in FSCIL task and NTK properties, SparK emerges as our preferred choice.

### B. Better Alignment: Margin-based Loss

In Sec. IV, our mixup strategy addresses the rigidity in class-level combinations, fostering enriched interactions for

the FSCIL learner across various virtual classes, thereby increasing the number of base class samples  $N$  and reducing the generalization loss  $L_D(f^*)$  as described in Theorem 3. Yet, this strategy also introduces certain side effects, namely, making traditional cross-entropy loss less effective in scenarios with a large number of classes [28], [29]. However, as highlighted in Eq. (3), alignment plays a crucial role in NTK dynamics and model generalization. Hence, to achieve more effective logit-label alignment, we replace cross-entropy loss with a margin-based loss [29], [45]. The fundamental structure of our margin-based softmax loss is outlined as follows:

$$\mathcal{L}_{logits} = -\log \frac{e^{sP(\cos \theta_{y_i})}}{e^{sP(\cos \theta_{y_i})} + \sum_{j \neq y_i}^n e^{sN(t, \cos \theta_j)}}, \quad (12)$$

Here,  $\theta_{y_i}$  and  $\theta_j$  represent the cosine similarities for the  $i$ -th and  $j$ -th class prototypes.  $P(\cdot)$  and  $N(\cdot)$  adjust positive and negative cosine similarities, respectively.

Furthermore, since the mixup mechanism’s inherent randomness in creating virtual classes, it can easily lead to an imbalance between virtual and real classes, which presents a significant challenge for margin-based loss. To counteract this, we adopt curriculum learning concepts [46], which involve adaptive alterations to  $P(\cdot)$  and  $N(\cdot)$ , as follows:

$$N(*) = \begin{cases} \cos \theta_j, & \varepsilon \geq 0 \\ \cos \theta_j(t + \cos \theta_j), & \varepsilon < 0, \end{cases} \quad (13)$$

$$P(*) = \begin{cases} \cos \theta_{y_i} \cos m - \cos^2 \theta_{y_i} \sin m, & \varepsilon \geq 0 \\ \cos(\theta_{y_i} + m) + m \sin m, & \varepsilon < 0, \end{cases} \quad (14)$$

where  $\varepsilon = \cos(\theta_i + m) - \cos \theta_j$  embodies the threshold,  $t$  is the mean logits updated via EMA mechanism over each batch, and  $m$  designates a predetermined, constant margin.

Through this refined design, training begins by deemphasizing negative samples, setting the initial value of  $t$  to zero, while simultaneously accentuating positive samples through the incorporation of  $m$ . As training progresses and reaches the desired performance, indicated by  $\varepsilon \geq 0$ ,  $t$  is incrementally increased to shift the model’s focus towards hard samples in positive classes. When certain classes achieve the target performance, we activate a suppression mechanism for highly accurate positive samples, thereby redirecting focus to less accurate ones. This recalibration ensures balanced performance across all class domains.

Ultimately, this adaptive optimization not only addresses the class weight imbalance but also significantly optimizes NTK dynamic outputs, as detailed in Sec. VI-H and VI-D.

### C. Refine NTK eigenvalues: Dual NTK Regularization

After ensuring the NTK dynamics reach an optimal state, according to Theorem 3, we need to further refine the eigenvalue distribution to avoid excessively large or small NTK eigenvalues, ensuring a stable NTK matrix is presented. However, as mentioned earlier, the computational burden associated with the NTK approximation in ConvNets challenges the limits of contemporary hardware. To address this, we adopt a compromise strategy, implementing dual NTK regularization that is specifically tailored to convolutional and linear layers.

This strategy delicately refines the NTK matrix, both indirectly and directly, by intervening in and tightening the NTK’s eigenvalue distribution. The details of the associated composite losses are provided below:

$$\mathcal{L}_{reg} = \mathcal{L}_{conv\_reg} + \mathcal{L}_{lin\_reg} \quad (15)$$

To ensure a slower eigenvalue decay in convolutional layers, we implement spectral regularization on their weights [16], [36]. Furthermore, to reduce the computational overhead associated with large-scale weight calculations, we employ Singular Value Decomposition (SVD) to decompose the weights. The detailed formulation is as follows:

$$\mathcal{L}_{conv\_reg} = \alpha \cdot \sum_{c \in f} \frac{\varphi_{max}^c}{\varphi_{min}^c}, \quad (16)$$

where  $\alpha$  is a hyperparameter,  $\varphi$  denotes the SVD function, and  $c$  is each convolutional weight in the ConvNet.

Conversely, for the additional linear layers, simplification is not necessary. Inspired by self-supervised linear evaluation studies [38], [41], [42], [44], we directly compute their NTK matrix and impose constraints on the eigenvalue distribution. Moreover, acknowledging the NTK’s inherent property—the optimal NTK stabilizes into a constant matrix irrespective of inputs after optimization—we concentrate on refining the stability of eigenvalue fluctuations in each batch, aiming to maintain relative consistency during optimization. Consequently, we devise a regularization loss to control the variance of these NTK eigenvalues:

$$\mathcal{L}_{lin\_reg} = \beta \cdot \frac{\sigma_{max}(\Phi_{linear}) - \sigma_{min}(\Phi_{linear})}{\sigma'_{max}(\Phi_{linear}) - \sigma'_{min}(\Phi_{linear})}, \quad (17)$$

where  $\Phi_{linear}$  denotes the linear layer’s NTK matrix,  $\beta$  symbolizes the hyperparameter governing the NTK eigenvalue fluctuation, while  $\sigma(\cdot)$  and  $\sigma'(\cdot)$  refer to the eigenvalues of the current and preceding batches respectively.

**Optimization:** Overall, our NTK-FSCIL adeptly navigates NTK convergence and NTK-related generalization loss through a three-stage process: SparK-based self-supervised pre-training on the base session, fully supervised FSCIL optimization on the base session and NCM testing on incremental sessions. During the crucial FSCIL optimization phase, the FSCIL learner is optimized through meta-learning, utilizing the sum of Eq. (10) and Eq. (15), ensuring optimal NTK convergence, NTK dynamics and minimal generalization loss.

## VI. EXPERIMENTS

In the experimental section, we commence with a detailed overview of the utilized datasets, as delineated in Sec. VI-A. This foundational step sets the stage for a series of experiments conducted on the most prominent FSCIL methods, meticulously validating the rationale and efficacy of each component. These components include the impact of convolutional network width on FSCIL performance as explored in Sec. VI-B, the influence of self-supervised pre-training (i.e., the initialization  $f_0^*(x)$ ) on FSCIL performance detailed in Sec. VI-C, the effect of logit-label alignment (i.e.,  $Y - f_0^*(X)$ )

Dataset	$C^{base}$	$N_{base}$	$C^{inc}$	#Inc.	Shots	Resolution
CIFAR100 [47]	60	30000	40	8	5	32×32
miniImageNet [49]	60	30000	40	8	5	84×84
CUB200 [48]	100	3000	100	10	5	224×224
ImageNet100 [50]	60	77352	40	8	5	112×112

TABLE I: Statistics of benchmarks datasets.  $C^{base}$ : number of classes in base session.  $C^{inc}$ : total number of classes in incremental sessions. #Inc.: number of incremental sessions. Shots: training shots for incremental sessions.  $N_{base}$ : number of samples in base session.

on FSCIL performance as discussed in Sec. VI-D, and the impact of expanding virtual classes, corresponding to  $N$  in Theorem 3, on outcomes as examined in Sec. VI-E.

Subsequent to these foundational experiments, we conduct comparative and analytical evaluations between our comprehensive approach and the latest methodologies in the field, supplemented by detailed ablation studies. This analytical journey culminates in a quantitative assessment of the eigenvalue distribution within the NTK matrix, alongside the visualization of embeddings through t-SNE plots, vividly illustrating NTK characteristics and model generalization capabilities.

#### A. Experimental Setup

**Datasets and Splits:** Our method is evaluated on multiple datasets: CIFAR100 [47] (consisting of 60,000 images across 100 classes), CUB200-2011 [48] (featuring 200 bird species classes), miniImageNet [49] (a subset of ImageNet-1K with 100 classes at reduced resolution) and ImageNet100 [50] (comprising 100 classes selected from ImageNet-1K). For CIFAR100, miniImageNet, and ImageNet100, we partition the classes into two sets: 60 base classes and 40 incremental classes. The latter are further divided into eight 5-way 5-shot tasks. In the case of CUB200, we have 100 base classes and 100 incremental classes, organized into ten 10-way 5-shot tasks. Our training splits align with those used in previous work [24], except for ImageNet100, which follows the splits introduced in [28]. More detailed content is shown in Tab. I.

#### B. Impacts of Network Width in FSCIL

In this subsection, we assess how network width influences FSCIL performance. Specifically, we select two methods, i.e., CEC [4] and ALICE [29], for evaluation by gradually widening the backbone. As shown in Fig. 2, an expansion in network width leads to a gradual enhancement in accuracy across sessions, providing additional evidence that widening the network improves its generalization. However, excessively increasing the width of the network poses significant challenges to optimization. Hence, unless stated otherwise, our default backbone is ResNet-18×2 (‘width128’ in Fig. 2), with doubled convolutional block widths.

Next, we aim to clearly demonstrate the impact of varying the width of individual convolutional layer on FSCIL performance. Using a ConvNet with doubled width as our baseline, we experimentally modify the width of specific layers and observe the resulting changes in FSCIL performance. These experiments are conducted using various ResNet architectures

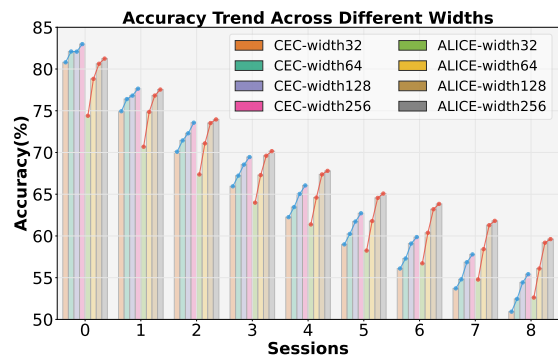


Fig. 2: The FSCIL performance on CIFAR100 across different widths in ResNet-18, employing the CEC [4] and ALICE [29].

on the CIFAR100 dataset to ensure efficient and informative outcomes. Table II provides a detailed analysis of the effects of varying the width of each convolutional layer on FSCIL performance. The data suggests a direct correlation: **as the width of these layers increases, FSCIL efficacy consistently improves**. This enhancement is observed not only when the entire ConvNet is widened but also when individual convolutional layer is selectively widened.

Subsequently, we extend this width modification approach to other members of the ResNet family, including ResNet-12, ResNet-20, ResNet-34 and ConvNext-tiny, conducting similar experiments on CIFAR100 as done with ResNet-18. The detailed outcomes of these experiments are presented in Fig. 3. These results consistently demonstrate that, irrespective of the specific CNN architecture, the generalization capabilities in incremental sessions are positively influenced by the width of the convolutional layers. The wider these layers, the better the performance in terms of generalization and FSCIL. These findings corroborate the NTK theory’s proposition regarding the relationship between a network’s width and its generalization ability, even within different CNN architectures.

#### C. Exploring Self-supervised Pre-training

In this subsection, we explicate and scrutinize the related experimental specifics and outcomes associated with the self-supervised pre-training component.

**CEC:** In assessing CEC’s performance, we exclude components such as the continually evolved classifier and the fine-tuning post pre-training, opting instead for the ‘autoaugment’ image transformation. The performance analysis, as detailed in Table III, involves six distinct self-supervised methodologies, excluding SimSiam [40] and SwAV [37] due to non-convergence on CIFAR100. The results indicate that self-supervised pre-training on base classes does not consistently enhance FSCIL performance for ConvNets in CEC. Only DINO [38], SparK [44] and MoCo-v3 [42] demonstrate positive results, whereas simCLR [39] and BYOL [43] show negative effects. This disparity may stem from the reliance of some self-supervised algorithms on contrastive learning and hand-crafted view transformations, which can lead to representation collapse in ConvNets, especially given CIFAR100’s

ResNet-18	CEC	ALICE	ResNet-18	CEC	ALICE
32⇒256⇒512⇒1024	81.2→53.9	79.4→58.0	128⇒64⇒512⇒1024	81.1→53.1	78.8→57.3
64⇒256⇒512⇒1024	81.6→53.6	80.0→58.0	128⇒128⇒512⇒1024	81.8→54.2	79.6→58.2
<b>128⇒256⇒512⇒1024</b>	<b>82.1→54.4</b>	<b>80.6→58.2</b>	<b>128⇒256⇒512⇒1024</b>	<b>82.1→54.4</b>	<b>80.6→58.2</b>
256⇒256⇒512⇒1024	82.3→54.7	80.7→58.2	128⇒512⇒512⇒1024	83.0→54.5	80.6→58.6

ResNet-18	CEC	ALICE	ResNet-18	CEC	ALICE
128⇒256⇒128⇒1024	81.3→52.7	78.8→57.2	128⇒256⇒512⇒256	84.7→54.9	79.7→57.4
128⇒256⇒256⇒1024	81.6→53.4	79.4→57.7	128⇒256⇒512⇒512	83.8→54.7	80.6→58.1
<b>128⇒256⇒512⇒1024</b>	<b>82.1→54.4</b>	<b>80.6→58.2</b>	<b>128⇒256⇒512⇒1024</b>	<b>82.1→54.4</b>	<b>80.6→58.2</b>
128⇒256⇒1024⇒1024	83.0→54.9	80.4→58.9	128⇒256⇒512⇒2048	80.6→52.3	80.3→58.7

TABLE II: The FSCIL performance on **CIFAR100** using ResNet-18 with varying widths of convolutional layers is presented. The baseline is indicated in bold, and the performance is measured solely by the accuracies in the base and final sessions.

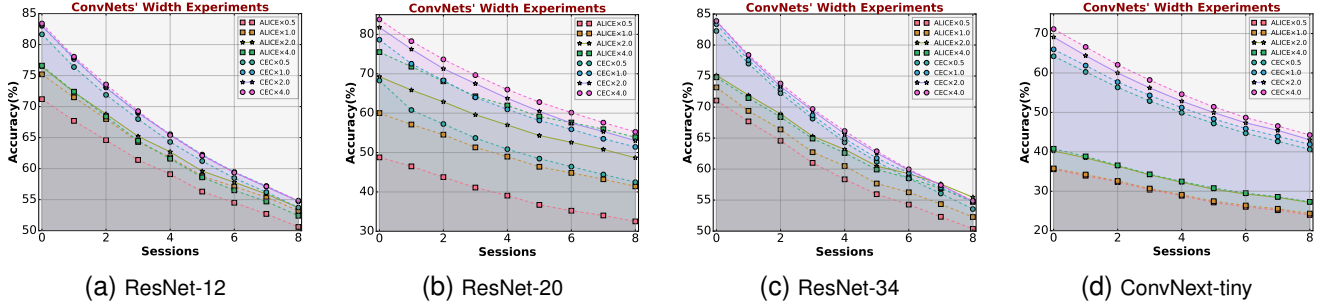


Fig. 3: This figure elucidates the FSCIL results of four different ConvNets (a.k.a. ResNet-12, ResNet-20, ResNet-34 and ConvNext), grounded on CEC and ALICE, following different width expansions on **CIFAR100**.

small image size. Such issues seem less prevalent in generative methods like masked image modeling.

**ALICE:** ALICE undergoes similar adaptations to CEC, including the removal of the 128-dimensional fully-connected layer from the backbone, reduction in mix-up volume, abandonment of the dual-branch training model, and discontinuation of balanced testing. Furthermore, ALICE’s outcomes, as detailed in Table IV, align with those observed in CEC. The performance of contrastive learning methodologies in FSCIL is notably inconsistent, with only BYOL showing slight improvements. In contrast, generative strategies based on masked image modeling, particularly SparK, consistently perform well. This supports our earlier hypothesis and suggests the reliability of these strategies from a different perspective.

In the spirit of rigorous scientific investigation, we extend our experiments to equivalent-sized Transformer-based models. Traditionally, these models are perceived as less effective than ConvNets in small datasets and few-shot tasks. However, our results show that with self-supervised pre-training, Transformers significantly close the performance gap, mirroring the results of the original CEC. This intriguing finding suggests that Transformer-based models may approach or even match ConvNets’ efficiency in few-shot scenarios, presenting an exciting avenue for future research.

#### D. Better Logit-Label Alignment

Drawing from the findings of [29], we delve into the performance of various loss functions, placing particular emphasis on those rooted in margin-based losses. More detailed results are presented in Table V. Our empirical analysis uncovers significant performance limitations when solely relying on

the traditional cross-entropy loss. Delving deeper, it becomes apparent that margin-based losses possess inherent advantages in handling a vast number of classes in the class extension mechanism. Among these margin-based losses, curricular alignment stands out significantly. This is largely attributed to its incorporation of the curriculum learning philosophy, mirroring the human education process of transitioning from simple to complex. It effectively balances the relationship between easy and hard samples and further alleviates the class imbalance issues introduced by the mixup mechanism. Furthermore, compared to other margin-based losses, our curricular alignment, despite lagging in base session accuracy, excels in incremental session accuracies. This indicates that it effectively learns from virtual classes, potentially reducing performance on real classes to some extent, but in turn, achieving better model generalization.

For hyperparameters  $s$  and  $m$ , our settings are closely aligned with those used in ALICE [29]. Specifically, for CIFAR100 and *miniImageNet*, we set  $s$  to 15.0 and  $m$  to 0.1. For datasets with larger image size and more complex information, such as CUB200 and ImageNet100, we adjust  $s$  to 25.0 while keeping  $m$  at 0.1, to accommodate the need for greater separation between positive and negative classes.

#### E. Exploring Logits Diversity in Meta-Learning

In FSCIL, the prevailing approaches often leverage the mix-up mechanism for class extension, directly merging two images [7], [29]. In this subsection, we delve into the nuanced variations of this mechanism. To investigate the impact of virtual classes generated by different mixup mechanisms on logits diversity, and further explore their effect on model

Method	Backbone	Acc. in each session (%) $\uparrow$								PD $\downarrow$	
		0	1	2	3	4	5	6	7		8
CEC [4]	ResNet-20	73.1	68.9	65.3	61.2	58.1	55.6	53.2	51.3	49.1	24.0
CEC* [4]	ResNet-20	79.0	73.1	68.8	64.8	61.4	58.3	56.0	53.8	51.7	27.3
CEC* [4]	ResNet-18 $\times$ 2	85.3	79.7	<b>74.9</b>	70.6	66.9	<b>63.8</b>	<b>61.3</b>	<b>58.7</b>	55.2	30.1
CEC* [4]	ViT-tiny	54.9	47.6	44.7	42.2	39.8	37.7	36.1	35.0	33.5	<b>21.4</b>
CEC* [4]	ViT-small	58.0	50.1	47.4	44.5	42.2	40.2	38.3	37.0	35.5	22.5
DINO [38]	ResNet-18 $\times$ 2	<b>85.8</b>	<b>80.1</b>	<b>75.1</b>	70.1	<b>67.0</b>	63.7	61.0	58.6	<b>56.0</b>	29.8
DINO [38]	ViT-tiny	75.0	69.8	65.2	61.1	57.8	54.6	51.8	49.6	47.4	<b>22.4</b>
DINO [38]	ViT-small	67.8	63.0	58.8	55.1	51.9	49.1	46.6	44.5	42.6	25.2
MAE [41]	ViT-tiny	78.6	73.8	69.1	64.9	61.3	58.3	55.4	53.0	50.4	28.2
MAE [41]	ViT-small	78.6	73.2	68.6	64.5	61.0	57.9	55.2	52.7	50.3	28.3
SparK [44]	ResNet-18 $\times$ 2	<b>85.5</b>	<b>80.0</b>	<b>75.1</b>	<b>70.8</b>	<b>67.1</b>	<b>63.8</b>	60.9	58.6	<b>56.2</b>	29.3
MoCo-v3 [42]	ResNet-18 $\times$ 2	<b>85.5</b>	79.8	74.7	<b>70.7</b>	67.0	<b>63.9</b>	<b>61.1</b>	<b>58.9</b>	<b>56.2</b>	29.3
MoCo-v3 [42]	ViT-tiny	69.4	64.8	60.9	57.3	54.0	51.3	48.8	46.5	51.7	28.1
MoCo-v3 [42]	ViT-small	74.1	69.6	65.9	62.0	58.8	55.9	53.4	51.3	49.2	24.9
simCLR [39]	ResNet-18 $\times$ 2	81.3	76.0	71.4	67.3	63.6	60.4	57.9	55.5	53.0	25.8
simCLR [39]	ViT-tiny	78.5	73.5	68.7	64.8	61.1	57.9	55.0	52.6	50.2	28.3
simCLR [39]	ViT-small	78.4	72.8	68.2	63.9	60.3	57.2	54.5	52.1	49.8	28.6
BYOL [43]	ResNet-18 $\times$ 2	82.0	76.9	72.1	68.2	64.5	61.5	59.0	56.6	54.1	27.9
BYOL [43]	ViT-tiny	66.2	59.6	56.1	52.7	50.1	47.8	45.6	44.0	42.3	23.9
BYOL [43]	ViT-small	66.1	60.0	56.5	53.1	50.3	47.8	45.5	43.4	41.7	24.4

TABLE III: The performance gleaned from various self-supervised learners on **CIFAR100**, anchored on **CEC** and the modified **CEC\***. The red-bolded segments represent the optimal results, while the blue-bolded segments represent suboptimal results.

Method	Backbone	Acc. in each session (%) $\uparrow$								PD $\downarrow$	
		0	1	2	3	4	5	6	7		8
ALICE [29]	ResNet-18	79.0	70.5	67.1	63.4	61.2	59.2	58.1	56.3	54.1	24.9
ALICE* [29]	ResNet-18	78.8	75.2	72.3	68.7	65.5	62.1	60.7	58.3	56.6	22.2
ALICE* [4]	ResNet-18 $\times$ 2	80.9	76.9	73.6	<b>69.9</b>	66.9	63.9	<b>62.5</b>	60.4	<b>58.3</b>	22.6
ALICE* [4]	ViT-tiny	58.7	55.4	52.3	49.0	46.8	44.4	42.4	40.8	39.1	<b>19.6</b>
ALICE* [4]	ViT-small	62.4	58.5	55.2	51.8	49.5	46.8	44.8	43.1	41.4	21.0
DINO [38]	ResNet-18 $\times$ 2	<b>84.7</b>	<b>79.1</b>	<b>74.9</b>	<b>70.3</b>	67.2	64.1	62.0	59.9	57.8	26.9
DINO [38]	ViT-tiny	82.7	76.9	71.9	67.4	63.9	60.7	57.7	55.1	52.8	29.9
DINO [38]	ViT-small	71.8	67.0	62.8	58.8	55.6	52.5	50.1	48.0	45.9	25.9
MAE [41]	ViT-tiny	81.9	76.7	71.7	67.5	64.2	60.9	58.1	55.5	53.2	28.7
MAE [41]	ViT-small	81.5	76.4	71.3	67.1	63.5	60.3	57.4	54.9	52.7	28.8
SparK [44]	ResNet-18 $\times$ 2	<b>83.6</b>	<b>77.7</b>	73.7	69.8	<b>67.4</b>	<b>64.6</b>	<b>63.0</b>	<b>61.0</b>	<b>58.8</b>	24.8
MoCo-v3 [42]	ResNet-18 $\times$ 2	82.4	77.5	73.3	68.9	66.2	63.1	60.9	58.8	56.8	25.6
MoCo-v3 [42]	ViT-tiny	78.7	73.4	68.7	64.7	61.1	57.8	55.2	52.8	50.5	28.2
MoCo-v3 [42]	ViT-small	78.4	73.1	68.4	64.0	60.3	57.3	54.5	52.1	49.8	28.6
simCLR [39]	ResNet-18 $\times$ 2	74.1	70.4	67.3	63.8	61.2	58.2	56.7	55.2	53.1	21.0
simCLR [39]	ViT-tiny	80.7	75.7	70.9	66.4	62.8	59.5	56.5	53.9	51.7	29.0
simCLR [39]	ViT-small	79.8	74.8	69.9	65.6	62.1	58.8	56.0	53.5	51.3	28.5
BYOL [43]	ResNet-18 $\times$ 2	82.9	<b>77.7</b>	<b>73.9</b>	69.8	<b>67.3</b>	<b>64.5</b>	<b>63.0</b>	<b>61.1</b>	<b>58.8</b>	24.1
BYOL [43]	ViT-tiny	56.9	53.5	50.4	47.3	45.0	42.7	40.7	39.0	37.2	<b>19.7</b>
BYOL [43]	ViT-small	55.5	52.0	48.8	45.4	43.2	40.8	38.9	37.6	35.9	<b>19.6</b>

TABLE IV: The performance from various self-supervised learners on **CIFAR100**, anchored on **ALICE** and the modified **ALICE\***. The red-bolded segments represent the optimal results, while the blue-bolded segments represent suboptimal results.

generalization, we employ the harmonic mean for an intuitive representation.

$$H = \frac{2 \times Base\ Acc \times Incremental\ Acc}{Base\ Acc + Incremental\ Acc}. \quad (18)$$

We conduct experiments with various mixup mechanisms on CIFAR100, and the results are displayed in Table VI. As shown in Table VI, methods that perform mixup operations globally on images produce better virtual samples and more flexible logit combinations, resulting in improved base session accuracy and harmonic mean. However, mixup methods involving image transformations fail to alleviate the rigid logit combinations in meta-learning. This could be due to the small image size of CIFAR100, where overly complex image transformations might irreversibly damage the original information and generate unrealistic virtual samples.

### F. Comparison with State-of-the-Art

In this subsection, we report the primary results for CIFAR100 in Tab. VII, *miniImageNet* in Tab. VIII, CUB200 in Tab. IX, and ImageNet100 in Tab. X. From the results, we observe that our NTK-FSCIL consistently outperforms its competitors. It exhibits superior end-session accuracy and an admirable PD, which represents the difference between initial and final session accuracies. A reduced PD value suggests enhanced anti-amnesia capability, while an elevated end-session accuracy indicates advanced generalization across incremental sessions. For instance, our method achieves a significant 8.2% improvement in end-session accuracy and 11.4% improvement in PD over NC-FSCIL on CIFAR100, underscoring its exceptional generalization and anti-amnesia capabilities. Furthermore, similar outcomes are also observed on other datasets. For the end-session accuracy on *miniImageNet* and ImageNet100, our NTK-FSCIL surpasses the nearest competi-



Classification Loss	Acc. in each session (%) $\uparrow$								
	0	1	2	3	4	5	6	7	8
<b>CE</b>	24.5	23.1	21.4	19.9	19.1	18.1	17.3	16.7	15.9
<b>ArcFace</b>	76.5	71.2	67.4	63.5	60.6	57.7	56.1	54.2	52.1
<b>CosFace</b>	77.0	71.9	67.1	63.2	60.8	57.9	56.2	54.3	52.2
<b>Curricular</b>	75.5	71.7	68.2	64.5	61.9	58.9	57.5	55.6	53.2

TABLE V: The notations **CE**, **ArcFace**, **CosFace** and **Curricular** correspond to Cross Entropy Loss, ArcFace Loss in [51], CosFace Loss in [52] and Curricular Loss respectively. All experiments are implemented on the ALICE [29] framework.

Methods	Acc. in each session (%) $\uparrow$									Base Acc.	Incremental Acc.	Harmonic Mean
	0	1	2	3	4	5	6	7	8			
<b>Mix-up</b> [53]	84.2	79.7	76.1	71.8	69.0	66.4	64.8	62.9	60.6	84.2	37.8	50.5
<b>CutMix</b> [54]	85.1	80.0	76.0	71.4	68.7	65.7	64.2	62.3	60.2	85.1	36.2	49.1
<b>AugMix</b> [55]	80.8	76.8	73.2	69.2	66.3	63.1	61.7	59.9	57.8	80.8	33.3	46.0
<b>PuzzleMix</b> [56]	84.4	79.9	76.6	72.3	69.6	66.7	65.0	63.1	61.0	84.4	37.2	50.1

TABLE VI: Average accuracy across base and incremental sessions using different mix-up methods, with their harmonic mean.

Method	Backbone	Params	FLOPs	Acc. in each session (%) $\uparrow$										PD $\downarrow$
				0	1	2	3	4	5	6	7	8		
iCaRL [1]	ResNet-32	0.47M	0.07G	64.1	53.3	41.7	34.1	27.9	25.1	20.4	15.5	13.7	50.4	
TOPIC [24]	ResNet-18	11.17M	0.56G	64.1	55.9	47.1	45.2	40.1	36.4	34.0	31.6	29.4	34.7	
CEC [4]	ResNet-20	0.27M	0.04G	73.1	68.9	65.3	61.2	58.1	55.6	53.2	51.3	49.1	24.0	
LIMIT [5]	ResNet-20	0.27M	0.04G	73.0	70.8	67.5	63.4	60.0	56.9	54.8	52.2	49.9	23.1	
FACT [28]	ResNet-20	0.27M	0.04G	74.6	72.1	67.6	63.5	61.4	58.4	56.3	54.2	52.1	<b>22.5</b>	
ALICE [29]	ResNet-18	11.17M	0.56G	79.0	70.5	67.1	63.4	61.2	59.2	58.1	56.3	54.1	24.9	
GKEAL [59]	ResNet-20	0.27M	0.04G	74.0	70.5	67.0	63.1	60.0	57.3	55.5	53.4	51.4	<b>22.6</b>	
WaRP [60]	ResNet-20	0.27M	0.04G	80.3	75.9	71.9	67.6	64.4	61.3	59.2	57.1	54.7	25.6	
SoftNet [6]	ResNet-18	11.17M	0.56G	79.9	75.5	71.6	67.5	64.5	61.1	59.1	57.3	55.3	24.6	
NC-FSCIL [7]	ResNet-12	12.42M	0.53G	<b>82.5</b>	76.8	73.3	69.7	66.2	62.9	61.0	59.0	56.1	26.4	
<b>NTK-FSCIL</b>	ResNet-18	11.17M	0.56G	81.8	<b>77.3</b>	<b>74.3</b>	<b>69.8</b>	<b>67.1</b>	<b>64.2</b>	<b>62.9</b>	<b>61.1</b>	<b>58.7</b>	23.1	
<b>NTK-FSCIL</b>	ResNet-18 $\times$ 2	44.65M	2.22G	<b>84.4</b>	<b>79.9</b>	<b>76.6</b>	<b>72.3</b>	<b>69.6</b>	<b>66.7</b>	<b>65.0</b>	<b>63.1</b>	<b>61.0</b>	23.4	

TABLE VII: Performance evaluation on **CIFAR100** dataset within the context of a 5-way 5-shot class-incremental learning paradigm. The red-bolded segments represent the optimal results, while the blue-bolded segments represent suboptimal results.

tors, NC-FSCIL [7] and CEC [4], by 3% and 6.2%.

For CUB200, considering that most methodologies, such as those proposed by [4], [7], [29], leverage the pre-trained weights of ResNet-18, it becomes necessary to bypass both the widening and self-supervised modules to maintain a fair comparison. Despite this limitation, our partial implementation of NTK-FSCIL still demonstrates remarkable efficacy. Additionally, we have adopted two more efficient pre-trained weights, namely Swin Transformer [57] and ConvNeXt [58], which have achieved far superior FSCIL performance.

At its core, our NTK-FSCIL, grounded in the principles of the NTK to enhance model generalization, primarily evaluates its success through performance in incremental learning sessions. Here, it showcases superior results, placing it at the forefront of the field. This adeptness in managing incremental sessions further enables our NTK-FSCIL model to achieve prominent positions in the PD metric, illustrating its comprehensive and balanced performance across various measures.

### G. Ablation Study

To demonstrate the effectiveness of NTK-FSCIL’s components, we perform an ablation study, detailed in Tab. XI. Each experiment utilizes curricular alignment, the details of which are outlined in Sec. V-B. For additional insights into alignment strategies, refer to Sec. VI-D.

The evidence from Table XI and Sec. VI-B, Sec. VI-C, Sec. VI-D and Sec. VI-E clearly show that each component of our NTK-FSCIL substantially improves the FSCIL

learner’s generalization in incremental sessions. Our meta-learning strategy, targeting NTK convergence, either matches or exceeds the current pre-training and fine-tuning paradigm in both efficiency and convergence. Furthermore, our findings reveal that network expansion, as per Definition 1, notably enhances the FSCIL learner’s generalization, yielding an approximate 5.5% improvement in end-session accuracy. Moreover, initializing the NTK with self-supervised pre-training on the base session significantly boosts its potential, establishing pre-training as a key strategy for enhancing NTK stability and overall model generalization. Compared to the baseline of width expansion and meta-learning, it results in a significant 2.8% increase in end-session accuracy.

Alongside these components, implementing linear and convolutional NTK regularization also contributes to a significant uptick in end-session accuracy, by around 3.4%. Despite this performance enhancement, it’s important to acknowledge the resultant uptick in computational demands, predominantly from the increased gradient computations per batch. Nevertheless, the overall computational burden of our NTK-FSCIL approach remains comparatively modest, especially when juxtaposed with conventional NTK fitting methodologies, striking a balance between computational efficiency and enhanced performance outcomes.

### H. NTK Contributions

To measure model generalization during optimization, we randomly sample images from both base and incremental

Method	Backbone	Params	FLOPs	Acc. in each session (%) $\uparrow$								PD $\downarrow$	
				0	1	2	3	4	5	6	7		8
iCaRL [1]	ResNet-18	11.17M	3.94G	61.3	46.3	42.9	37.6	30.5	24.0	20.9	18.8	17.2	44.1
TOPIC [24]	ResNet-18	11.17M	3.94G	61.3	50.1	45.2	41.2	37.5	35.5	32.2	29.5	24.4	36.9
CEC [4]	ResNet-18	11.17M	3.94G	72.0	66.8	63.0	59.4	56.7	53.7	51.2	49.2	47.6	24.4
LIMIT [5]	ResNet-18	11.17M	3.94G	71.9	67.9	63.6	60.2	57.3	54.3	52.0	50.0	48.4	23.5
FACT [28]	ResNet-18	11.17M	3.94G	72.6	69.6	66.4	62.8	60.6	57.3	54.3	52.2	50.5	22.1
ALICE [29]	ResNet-18	11.17M	3.94G	80.6	70.6	67.4	64.5	62.5	60.0	57.8	56.8	55.7	24.9
GKEAL [59]	ResNet-18	11.17M	3.94G	73.6	68.9	65.3	62.3	59.4	56.7	54.2	52.6	51.3	<b>22.3</b>
WaRP [60]	ResNet-18	11.17M	3.94G	73.0	68.1	64.3	61.3	58.6	56.1	53.4	51.7	50.7	<b>22.3</b>
SoftNet [6]	ResNet-18	11.17M	3.94G	79.4	74.3	69.9	66.2	63.4	60.8	57.6	55.7	54.3	25.1
NC-FSCIL [7]	ResNet-12	12.42M	3.53G	<b>84.0</b>	<b>76.8</b>	<b>72.0</b>	67.8	<b>66.4</b>	<b>64.0</b>	<b>61.5</b>	59.5	58.3	25.7
NTK-FSCIL	ResNet-18	11.17M	3.94G	80.0	75.5	71.6	<b>68.6</b>	<b>66.4</b>	<b>64.0</b>	61.3	<b>59.9</b>	<b>58.8</b>	<b>21.2</b>
NTK-FSCIL	ResNet-18 $\times$ 2	44.65M	15.69G	<b>82.4</b>	<b>77.2</b>	<b>73.3</b>	<b>70.2</b>	<b>67.8</b>	<b>65.3</b>	<b>62.7</b>	<b>60.9</b>	<b>60.0</b>	22.4

TABLE VIII: Performance evaluation on *miniImageNet* dataset within the context of a 5-way 5-shot class-incremental learning paradigm. The red-bolded segments represent the optimal results, while the blue-bolded segments represent suboptimal results.

Method	Backbone	Params	FLOPs	Acc. in each session (%) $\uparrow$										PD $\downarrow$	
				0	1	2	3	4	5	6	7	8	9		10
iCaRL [1]	ResNet-18	11.17M	27.37G	68.7	52.7	48.6	44.2	36.6	29.5	27.8	26.3	24.0	23.9	21.2	47.5
TOPIC [24]	ResNet-18	11.17M	27.37G	68.7	62.5	54.8	50.0	45.3	41.4	38.4	35.4	32.2	28.3	26.3	42.4
CEC [4]	ResNet-18	11.17M	27.37G	75.9	71.9	68.5	63.5	62.4	58.3	57.7	55.8	54.8	53.5	52.3	23.6
LIMIT [5]	ResNet-18	11.17M	27.37G	76.3	74.2	<b>72.7</b>	69.2	68.8	65.6	63.6	62.7	61.5	60.4	58.4	17.9
FACT [28]	ResNet-18	11.17M	27.37G	75.9	73.2	70.8	66.1	65.6	62.2	61.7	59.8	58.4	57.9	56.9	19.0
ALICE [29]	ResNet-18	11.17M	27.37G	77.4	72.7	70.6	67.2	65.9	63.4	62.9	61.9	60.5	60.6	60.1	17.3
GKEAL [59]	ResNet-18	11.17M	27.37G	78.9	75.6	72.3	68.6	67.2	64.3	63.0	61.9	60.2	59.2	58.7	20.2
WaRP [60]	ResNet-18	11.17M	27.37G	77.7	74.2	70.8	66.9	65.0	62.6	61.4	59.9	58.0	57.8	57.0	20.7
SoftNet [6]	ResNet-18	11.17M	27.37G	78.1	74.6	71.3	67.5	65.1	62.4	60.8	59.2	57.4	57.1	56.6	21.5
NC-FSCIL [7]	ResNet-18	11.17M	27.37G	80.5	76.0	72.3	70.3	68.2	65.2	<b>64.4</b>	63.3	60.7	60.0	59.4	21.1
NTK-FSCIL	ResNet-18	11.17M	27.37G	78.1	75.0	72.0	68.6	67.1	64.6	63.6	62.7	61.1	61.0	60.4	17.9
NTK-FSCIL	Swin-Small	50.0M	8.7G	<b>84.0</b>	<b>81.8</b>	<b>80.1</b>	<b>77.4</b>	<b>76.6</b>	<b>74.6</b>	<b>74.6</b>	<b>74.4</b>	<b>74.0</b>	<b>73.9</b>	<b>73.6</b>	<b>10.4</b>
NTK-FSCIL	ConvNeXt-Base	88.6M	15.4G	<b>83.3</b>	<b>81.3</b>	<b>80.1</b>	<b>78.0</b>	<b>77.2</b>	<b>74.9</b>	<b>74.6</b>	<b>74.5</b>	<b>74.3</b>	<b>74.2</b>	<b>74.0</b>	<b>9.3</b>

TABLE IX: Performance evaluation on *CUB-200-2011* dataset within the context of a 10-way 5-shot class-incremental learning paradigm. The red-bolded segments represent the optimal results, while the blue-bolded segments represent suboptimal results.

Method	Backbone	Params	FLOPs	Acc. in each session (%) $\uparrow$								PD $\downarrow$	
				0	1	2	3	4	5	6	7		8
CEC* [4]	ResNet-18	11.17M	27.37G	<b>72.9</b>	66.0	62.8	60.3	56.8	54.0	52.8	52.3	50.0	22.9
ALICE* [29]	ResNet-18	11.17M	27.37G	68.8	63.2	60.0	57.1	53.4	50.3	48.5	47.7	45.5	23.3
NTK-FSCIL	ResNet-18	11.17M	27.37G	72.8	<b>68.9</b>	<b>65.5</b>	<b>63.0</b>	<b>58.9</b>	<b>56.2</b>	<b>54.4</b>	<b>53.4</b>	<b>51.1</b>	<b>21.7</b>
NTK-FSCIL	ResNet-18 $\times$ 2	44.65M	108.99G	<b>74.9</b>	<b>69.5</b>	<b>66.4</b>	<b>63.5</b>	<b>60.0</b>	<b>57.7</b>	<b>56.0</b>	<b>55.4</b>	<b>53.1</b>	<b>21.8</b>

TABLE X: Performance evaluation on *ImageNet100* dataset within the context of a 5-way 5-shot class-incremental learning paradigm. The red-bolded segments represent the optimal results, while the blue-bolded segments represent suboptimal results.

ML	WC	SSI	LNR	CSR	Acc. in each session (%) $\uparrow$								$\Delta_{last} \uparrow$	
					0	1	2	3	4	5	6	7		8
$\checkmark$					75.3	71.9	68.5	64.2	61.7	59.1	57.7	56.2	54.4	+0.0
$\checkmark$	$\checkmark$				79.2	75.4	72.0	67.9	65.4	62.7	61.2	59.6	57.4	+3.0
$\checkmark$	$\checkmark$	$\checkmark$			82.9	78.7	74.5	70.5	67.8	65.1	63.7	61.8	59.0	+4.6
$\checkmark$	$\checkmark$	$\checkmark$	$\checkmark$		83.3	78.7	75.2	71.0	67.7	65.1	63.5	61.6	59.5	+5.1
$\checkmark$	$\checkmark$	$\checkmark$	$\checkmark$	$\checkmark$	84.4	79.9	76.6	72.3	69.6	66.7	65.0	63.1	61.0	+6.6

TABLE XI: Ablation studies (%) on *CIFAR100* benchmark. Specifically, the symbols **ML**, **WC**, **SSI**, **LNR** and **CSR** represent Meta-Learning in Subsec. IV, Wider ConvNets in in Subsec. VI-B, Self-Supervised Initialization in Subsec. V-A, Linear NTK Regularization and Convolutional Spectral Regularization in Subsec. V-C, respectively. The  $\Delta_{last} \uparrow$  denotes the improvement over the first row’s scenario.

sessions. For GPU efficiency, we only compute the NTK matrix solely for the final nested linear layers. This allows us to scrutinize the linear operations, thereby providing insight into how the ultimate linear layers contribute to the model generalization. Following the construction of the NTK matrix, we monitor them in real time by evaluating the evolution of eigenvalues and the accuracy of the base session. The condition number of the NTK matrix is then computed as an indicator of its stability, in a manner analogous to Eq. (16), defined as the maximum-to-minimum eigenvalue ratio.

The detailed evolutionary trajectories, including changes in the minimum and maximum eigenvalues, condition number, and accuracy, are illustrated in Fig. 5. Interestingly, we observe a strong positive correlation between the eigenvalues of the NTK matrix and the accuracy. The NTK’s eigenvalues grad-

ually converge, maintaining a state of equilibrium, mirroring the trend of ascending and then stabilizing accuracy. Moreover, the condition number remains relatively stable, illustrating the gradual convergence and stability of the NTK matrix, thereby facilitating improved generalization.

To probe the impact of widening ConvNet, meta-learning, self-supervised pre-training, curricular alignment and dual NTK regularization on NTK properties, we conduct a comprehensive analysis on CIFAR100. We systematically omit each module one by one to observe the resulting shifts in the NTK’s eigenvalue distribution, as depicted in Fig. 4.

From Fig. 4a, Fig. 4b, Fig. 4c and Fig. 4d, it’s evident that Linear NTK Regularization, Convolutional NTK Regularization, Curricular Alignment and Self-supervised Pre-training play vital roles in ensuring NTK stability during

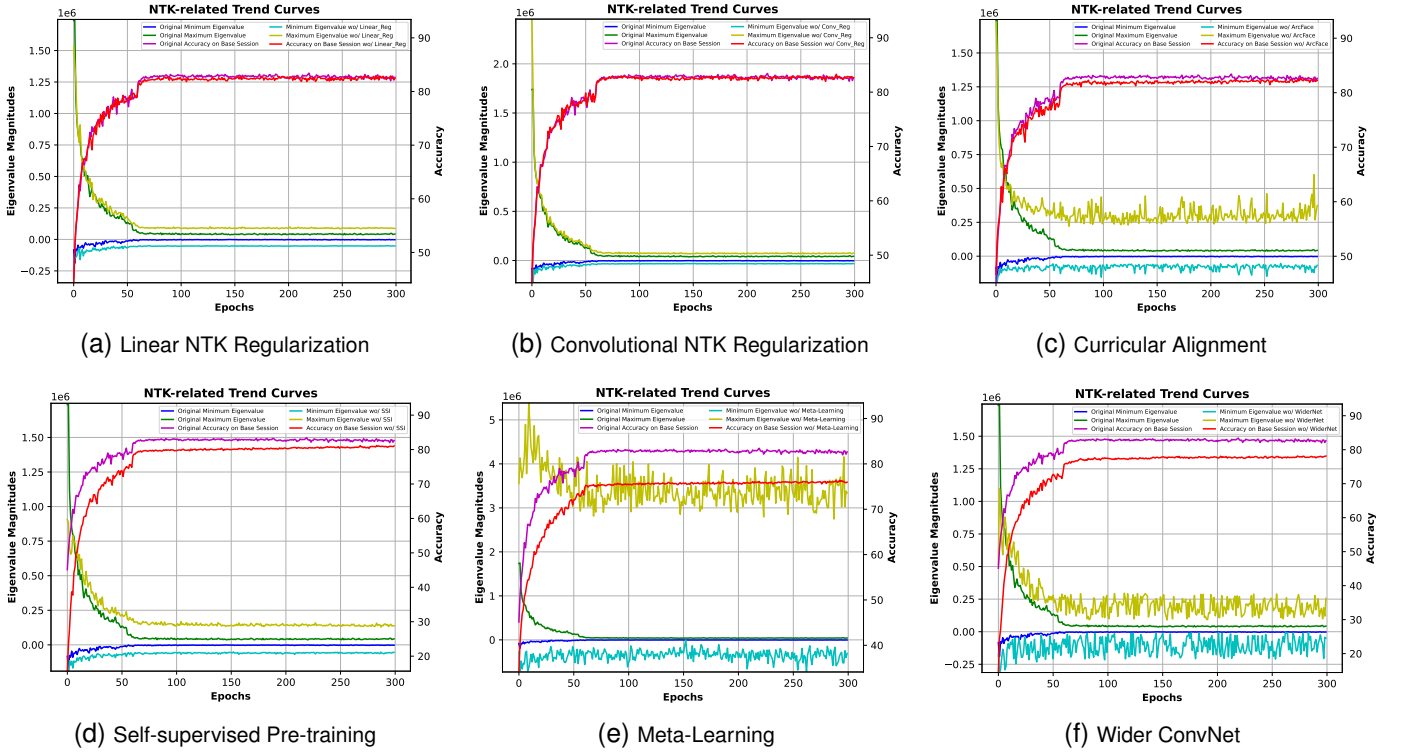


Fig. 4: Investigate the NTK dynamics post-elimination of Linear NTK Regularization, Convolutional NTK Regularization, Curricular Alignment, Meta-Learning and Wider ConvNet strategies.

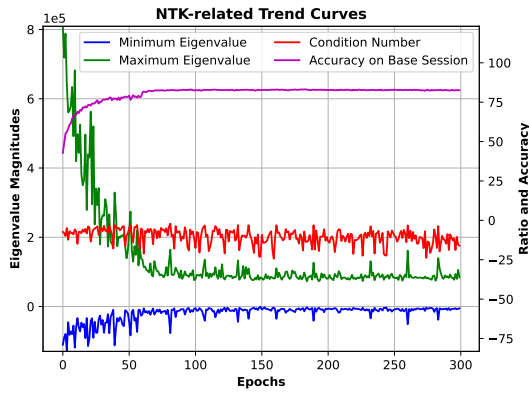


Fig. 5: NTK-related metrics and accuracy on the base session.

optimization. Omitting or altering any of these components leads to a markedly erratic NTK’s eigenvalue distribution, characterized by significant variations between the highest and lowest eigenvalues. Such instability negatively impacts the base session accuracy and hampers model generalization. Similarly, as shown in Fig. 4e and Fig. 4f, Meta-Learning and a Wider ConvNet are essential for NTK convergence. Their absence results in unpredictable fluctuations in the NTK eigenvalue distribution, with the maximum and minimum eigenvalues lacking a consistent path during optimization, further affecting model generalization.

In summary, each component within our NTK-FSCIL plays a critical role in ensuring the NTK’s convergence and stability during optimization. Their combined efforts enable our FSCIL learner to exhibit strong generalization capabilities at

the NTK theoretical level, leading to impressive performance in incremental sessions. Consequently, it not only improves overall FSCIL performance but also effectively mitigates the catastrophic forgetting problem.

### I. Visualization

To compellingly showcase the advantages of our NTK-FSCIL methodology, we employ t-SNE visualization to depict the embeddings generated by our optimized model, as illustrated in Fig. 6. Initially, we select five categories from the base session, with each category comprising 20 samples, as displayed in Fig. 6a. Following this, we enrich this dataset by adding four additional categories from subsequent incremental sessions, with each new category contributing 5 samples. This augmentation leads to a more detailed and insightful t-SNE visualization, as exhibited in Fig. 6b, which offers a clearer perspective on the optimized embedding space.

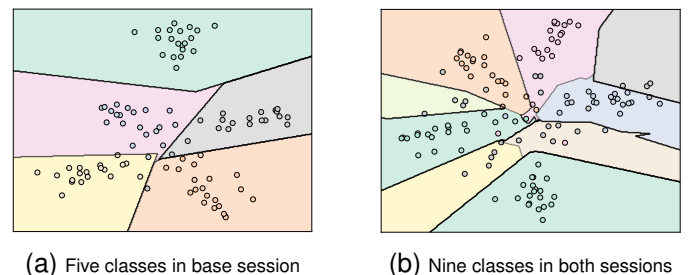


Fig. 6: t-SNE visualization of embeddings from randomly sampled instances in the base session and incremental sessions.

As demonstrated in Fig. 6, our NTK-FSCIL method distinctively segregates samples from both base and incremental sessions, showcasing enhanced separability and a clear testament to the model’s generalization capabilities. This visualization not only highlights the effectiveness of our approach in creating distinct representations for different categories but also underscores its ability to adapt and maintain performance across incremental learning phases.

## VII. CONCLUSION

Our research applies the Neural Tangents Kernel (NTK) theory to the FSCIL paradigm, establishing a robust correlation between model generalization capabilities and NTK convergence and NTK-related generalization loss. Through both theoretical and empirical analyses, we validate the significance of NTK in FSCIL generalization. Our NTK-FSCIL approach, emphasizing NTK matrix optimization, attains exceptional results on well-established FSCIL benchmarks.

## REFERENCES

- [1] S.-A. Rebuffi, A. Kolesnikov, G. Sperl, and C. H. Lampert, “icarl: Incremental classifier and representation learning,” in *Proceedings of the IEEE/CVF Conference on Computer Vision and Pattern Recognition*, 2017, pp. 2001–2010.
- [2] S. Yan, J. Xie, and X. He, “Der: Dynamically expandable representation for class incremental learning,” in *Proceedings of the IEEE/CVF Conference on Computer Vision and Pattern Recognition*, 2021, pp. 3014–3023.
- [3] A. Douillard, A. Ramé, G. Couairon, and M. Cord, “Dytox: Transformers for continual learning with dynamic token expansion,” in *Proceedings of the IEEE/CVF Conference on Computer Vision and Pattern Recognition*, 2022, pp. 9285–9295.
- [4] C. Zhang, N. Song, G. Lin, Y. Zheng, P. Pan, and Y. Xu, “Few-shot incremental learning with continually evolved classifiers,” in *Proceedings of the IEEE/CVF Conference on Computer Vision and Pattern Recognition*, 2021, pp. 12 455–12 464.
- [5] D.-W. Zhou, H.-J. Ye, L. Ma, D. Xie, S. Pu, and D.-C. Zhan, “Few-shot class-incremental learning by sampling multi-phase tasks,” *IEEE Transactions on Pattern Analysis and Machine Intelligence*, 2022.
- [6] J. Yoon, S. Madjid, S. J. Hwang, C.-D. Yoo *et al.*, “On the soft-subnetwork for few-shot class incremental learning,” in *International Conference on Learning Representations*. International Conference on Learning Representations, 2023.
- [7] Y. Yang, H. Yuan, X. Li, Z. Lin, P. Torr, and D. Tao, “Neural collapse inspired feature-classifier alignment for few-shot class-incremental learning,” in *International Conference on Learning Representations*, 2023.
- [8] R. Novak, J. Sohl-Dickstein, and S. S. Schoenholz, “Fast finite width neural tangent kernel,” in *International Conference on Machine Learning*. PMLR, 2022, pp. 17 018–17 044.
- [9] F. Cagnetta, A. Favero, and M. Wyart, “What can be learnt with wide convolutional neural networks?” in *International Conference on Machine Learning*. PMLR, 2022.
- [10] A. Jacot, F. Gabriel, and C. Hongler, “Neural tangent kernel: Convergence and generalization in neural networks,” *Advances in Neural Information Processing Systems*, vol. 31, 2018.
- [11] H. Wang, Y. Wang, R. Sun, and B. Li, “Global convergence of maml and theory-inspired neural architecture search for few-shot learning,” in *Proceedings of the IEEE/CVF Conference on Computer Vision and Pattern Recognition*, 2022, pp. 9797–9808.
- [12] F. Caron, F. Ayed, P. Jung, H. Lee, J. Lee, and H. Yang, “Over-parameterised shallow neural networks with asymmetrical node scaling: Global convergence guarantees and feature learning,” *arXiv preprint arXiv:2302.01002*, 2023.
- [13] S. S. Du, X. Zhai, B. Póczos, and A. Singh, “Gradient descent provably optimizes over-parameterized neural networks,” *arXiv preprint arXiv:1810.02054*, 2018.
- [14] D. Zou, Y. Cao, D. Zhou, and Q. Gu, “Stochastic gradient descent optimizes over-parameterized deep relu networks,” *arXiv preprint arXiv:1811.08888*, 2018.
- [15] Z. Allen-Zhu, Y. Li, and Z. Song, “A convergence theory for deep learning via over-parameterization,” in *International Conference on Machine Learning*. PMLR, 2019, pp. 242–252.
- [16] A. Wei, W. Hu, and J. Steinhardt, “More than a toy: Random matrix models predict how real-world neural representations generalize,” in *International Conference on Machine Learning*. PMLR, 2022, pp. 23 549–23 588.
- [17] D. Richards and I. Kuzborskij, “Stability & generalisation of gradient descent for shallow neural networks without the neural tangent kernel,” in *Advances in Neural Information Processing Systems*, A. Beygelzimer, Y. Dauphin, P. Liang, and J. W. Vaughan, Eds., 2021.
- [18] S. Bombari and M. Mondelli, “Stability, generalization and privacy: Precise analysis for random and ntk features,” *arXiv preprint arXiv:2305.12100*, 2023.
- [19] H. Taheri and C. Thrampoulidis, “Generalization and stability of interpolating neural networks with minimal width,” *arXiv preprint arXiv:2302.09235*, 2023.
- [20] R. M. Neal and R. M. Neal, “Priors for infinite networks,” *Bayesian Learning for Neural Networks*, pp. 29–53, 1996.
- [21] N. Le Roux and Y. Bengio, “Continuous neural networks,” in *Artificial Intelligence and Statistics*. PMLR, 2007, pp. 404–411.
- [22] T. Hazan and T. Jaakkola, “Steps toward deep kernel methods from infinite neural networks,” *arXiv preprint arXiv:1508.05133*, 2015.
- [23] S. Du and W. Hu, “Width provably matters in optimization for deep linear neural networks,” in *International Conference on Machine Learning*. PMLR, 2019, pp. 1655–1664.
- [24] X. Tao, X. Hong, X. Chang, S. Dong, X. Wei, and Y. Gong, “Few-shot class-incremental learning,” in *Proceedings of the IEEE/CVF Conference on Computer Vision and Pattern Recognition*, 2020, pp. 12 183–12 192.
- [25] G. Shi, J. Chen, W. Zhang, L.-M. Zhan, and X.-M. Wu, “Overcoming catastrophic forgetting in incremental few-shot learning by finding flat minima,” *Advances in Neural Information Processing Systems*, vol. 34, pp. 6747–6761, 2021.
- [26] M. Hersche, G. Karunaratne, G. Cherubini, L. Benini, A. Sebastian, and A. Rahimi, “Constrained few-shot class-incremental learning,” in *Proceedings of the IEEE/CVF Conference on Computer Vision and Pattern Recognition*, 2022, pp. 9057–9067.
- [27] Z. Ji, Z. Hou, X. Liu, Y. Pang, and X. Li, “Memorizing complementation network for few-shot class-incremental learning,” in *IEEE Transactions on Image Processing*, 2023, pp. 937–948.
- [28] D.-W. Zhou, F.-Y. Wang, H.-J. Ye, L. Ma, S. Pu, and D.-C. Zhan, “Forward compatible few-shot class-incremental learning,” in *Proceedings of the IEEE/CVF Conference on Computer Vision and Pattern Recognition*, 2022, pp. 9046–9056.
- [29] C. Peng, K. Zhao, T. Wang, M. Li, and B. C. Lovell, “Few-shot class-incremental learning from an open-set perspective,” in *European Conference on Computer Vision*. Springer, 2022, pp. 382–397.
- [30] J. Lee, L. Xiao, S. Schoenholz, Y. Bahri, R. Novak, J. Sohl-Dickstein, and J. Pennington, “Wide neural networks of any depth evolve as linear models under gradient descent,” *Advances in Neural Information Processing Systems*, vol. 32, 2019.
- [31] G. Yang, “Tensor programs ii: Neural tangent kernel for any architecture,” *arXiv preprint arXiv:2006.14548*, 2020.
- [32] A. Canatar, B. Bordelon, and C. Pehlevan, “Spectral bias and task-model alignment explain generalization in kernel regression and infinitely wide neural networks,” *Nature communications*, vol. 12, no. 1, p. 2914, 2021.
- [33] Q. Nguyen, M. Mondelli, and G. F. Montufar, “Tight bounds on the smallest eigenvalue of the neural tangent kernel for deep relu networks,” in *International Conference on Machine Learning*. PMLR, 2021, pp. 8119–8129.
- [34] M. Murray, H. Jin, B. Bowman, and G. Montufar, “Characterizing the spectrum of the ntk via a power series expansion,” *arXiv preprint arXiv:2211.07844*, 2022.
- [35] Z. Chi, L. Gu, H. Liu, Y. Wang, Y. Yu, and J. Tang, “Metafscil: a meta-learning approach for few-shot class incremental learning,” in *Proceedings of the IEEE/CVF Conference on Computer Vision and Pattern Recognition*, 2022, pp. 14 166–14 175.
- [36] C. Wei, J. D. Lee, Q. Liu, and T. Ma, “Regularization matters: Generalization and optimization of neural nets vs their induced kernel,” *Advances in Neural Information Processing Systems*, vol. 32, 2019.
- [37] M. Caron, I. Misra, J. Mairal, P. Goyal, P. Bojanowski, and A. Joulin, “Unsupervised learning of visual features by contrasting cluster assignments,” *Advances in Neural Information Processing Systems*, vol. 33, pp. 9912–9924, 2020.
- [38] M. Caron, H. Touvron, I. Misra, H. Jégou, J. Mairal, P. Bojanowski, and A. Joulin, “Emerging properties in self-supervised vision transformers,”

- in *Proceedings of the IEEE/CVF International Conference on Computer Vision*, 2021, pp. 9650–9660.
- [39] T. Chen, S. Kornblith, M. Norouzi, and G. Hinton, “A simple framework for contrastive learning of visual representations,” in *International Conference on Machine Learning*. PMLR, 2020, pp. 1597–1607.
- [40] X. Chen and K. He, “Exploring simple siamese representation learning,” in *Proceedings of the IEEE/CVF Conference on Computer Vision and Pattern Recognition*, 2021, pp. 15 750–15 758.
- [41] K. He, X. Chen, S. Xie, Y. Li, P. Dollár, and R. Girshick, “Masked autoencoders are scalable vision learners,” in *Proceedings of the IEEE/CVF Conference on Computer Vision and Pattern Recognition*, 2022, pp. 16 000–16 009.
- [42] X. Chen\*, S. Xie\*, and K. He, “An empirical study of training self-supervised vision transformers,” *arXiv preprint arXiv:2104.02057*, 2021.
- [43] J.-B. Grill, F. Strub, F. Altché, C. Tallec, P. Richemond, E. Buchatskaya, C. Doersch, B. Avila Pires, Z. Guo, M. Gheshlaghi Azar *et al.*, “Bootstrap your own latent—a new approach to self-supervised learning,” *Advances in Neural Information Processing Systems*, vol. 33, pp. 21 271–21 284, 2020.
- [44] K. Tian, Y. Jiang, qishuai diao, C. Lin, L. Wang, and Z. Yuan, “Designing BERT for convolutional networks: Sparse and hierarchical masked modeling,” in *International Conference on Learning Representations*, 2023. [Online]. Available: <https://openreview.net/forum?id=NRxydtWup1S>
- [45] Y. Zou, S. Zhang, Y. Li, and R. Li, “Margin-based few-shot class-incremental learning with class-level overfitting mitigation,” in *Advances in Neural Information Processing Systems*, A. H. Oh, A. Agarwal, D. Belgrave, and K. Cho, Eds., 2022.
- [46] Y. Huang, Y. Wang, Y. Tai, X. Liu, P. Shen, S. Li, J. Li, and F. Huang, “Curricularface: adaptive curriculum learning loss for deep face recognition,” in *Proceedings of the IEEE/CVF Conference on Computer Vision and Pattern Recognition*, 2020, pp. 5901–5910.
- [47] A. Krizhevsky, G. Hinton *et al.*, “Learning multiple layers of features from tiny images,” 2009.
- [48] C. Wah, S. Branson, P. Welinder, P. Perona, and S. Belongie, “The caltech-ucsd birds-200-2011 dataset,” 2011.
- [49] O. Russakovsky, J. Deng, H. Su, J. Krause, S. Satheesh, S. Ma, Z. Huang, A. Karpathy, A. Khosla, M. Bernstein, A. C. Berg, and L. Fei-Fei, “ImageNet Large Scale Visual Recognition Challenge,” *International Journal of Computer Vision (IJCV)*, vol. 115, no. 3, pp. 211–252, 2015.
- [50] Y. Wu, Y. Chen, L. Wang, Y. Ye, Z. Liu, Y. Guo, and Y. Fu, “Large scale incremental learning,” in *Proceedings of the IEEE/CVF Conference on Computer Vision and Pattern Recognition*, 2019, pp. 374–382.
- [51] J. Deng, J. Guo, N. Xue, and S. Zafeiriou, “Arcface: Additive angular margin loss for deep face recognition,” in *Proceedings of the IEEE/CVF Conference on Computer Vision and Pattern Recognition*, 2019, pp. 4690–4699.
- [52] H. Wang, Y. Wang, Z. Zhou, X. Ji, D. Gong, J. Zhou, Z. Li, and W. Liu, “Cosface: Large margin cosine loss for deep face recognition,” in *Proceedings of the IEEE/CVF Conference on Computer Vision and Pattern Recognition*, 2018, pp. 5265–5274.
- [53] H. Zhang, M. Cisse, Y. N. Dauphin, and D. Lopez-Paz, “mixup: Beyond empirical risk minimization,” in *International Conference on Learning Representations*, 2018. [Online]. Available: <https://openreview.net/forum?id=r1Ddp1-Rb>
- [54] S. Yun, D. Han, S. J. Oh, S. Chun, J. Choe, and Y. Yoo, “Cutmix: Regularization strategy to train strong classifiers with localizable features,” in *Proceedings of the IEEE/CVF International Conference on Computer Vision*, 2019, pp. 6023–6032.
- [55] D. Hendrycks\*, N. Mu\*, E. D. Cubuk, B. Zoph, J. Gilmer, and B. Lakshminarayanan, “Augmix: A simple method to improve robustness and uncertainty under data shift,” in *International Conference on Learning Representations*, 2020. [Online]. Available: <https://openreview.net/forum?id=S1gmrxFvB>
- [56] J.-H. Kim, W. Choo, and H. O. Song, “Puzzle mix: Exploiting saliency and local statistics for optimal mixup,” in *International Conference on Machine Learning*. PMLR, 2020, pp. 5275–5285.
- [57] Z. Liu, Y. Lin, Y. Cao, H. Hu, Y. Wei, Z. Zhang, S. Lin, and B. Guo, “Swin transformer: Hierarchical vision transformer using shifted windows,” in *Proceedings of the IEEE/CVF international conference on computer vision*, 2021, pp. 10 012–10 022.
- [58] Z. Liu, H. Mao, C.-Y. Wu, C. Feichtenhofer, T. Darrell, and S. Xie, “A convnet for the 2020s,” in *Proceedings of the IEEE/CVF conference on computer vision and pattern recognition*, 2022, pp. 11 976–11 986.
- [59] H. Zhuang, Z. Weng, R. He, Z. Lin, and Z. Zeng, “Gkeal: Gaussian kernel embedded analytic learning for few-shot class incremental task,”

in *Proceedings of the IEEE/CVF Conference on Computer Vision and Pattern Recognition*, 2023, pp. 7746–7755.

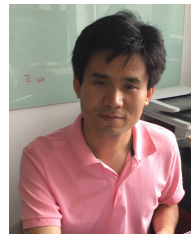
- [60] D.-Y. Kim, D.-J. Han, J. Seo, and J. Moon, “Warping the space: Weight space rotation for class-incremental few-shot learning,” in *International Conference on Learning Representations*, 2023. [Online]. Available: <https://openreview.net/forum?id=kPLzOfPFA2l>



**Jingren Liu** received the B.S. degree in Computer Science and Technology from Nanjing University of Finance and Economy, Nanjing, China, in 2019, and is currently working toward the PhD degree in the School of Electrical and Information Engineering, Tianjin University, Tianjin, China. His current research interests include continual learning, few shot learning, and prompt learning.



**Zhong Ji** received the Ph.D. degree in signal and information processing from Tianjin University, Tianjin, China, in 2008. He is currently a Professor with the School of Electrical and Information Engineering, Tianjin University. He has authored over 100 technical articles in refereed journals and proceedings. His current research interests include continual learning, few shot learning, and cross-modal analysis.



**YanWei Pang** received the Ph.D. degree in electronic engineering from the University of Science and Technology of China, Hefei, China, in 2004. He is currently a Professor with the School of Electrical and Information Engineering, Tianjin University, Tianjin, China. He has authored over 200 scientific papers. His current research interests include object detection and recognition, vision in bad weather, and computer vision.



**YunLong Yu** received the Ph.D. degree in information and communication engineering from Tianjin University, Tianjin, China, in 2019. He is currently a Distinguished Associate Researcher with the College of Information Science and Electronic Engineering, Zhejiang University, Hangzhou, China. His current research interests include machine learning and computer vision.